Journal of Catalysis 343 (2016) 133–146

Contents lists available at ScienceDirect

Journal of Catalysis

journal homepage: www.elsevier.com/locate/jcat

Pd/ZnO catalysts for direct CO_2 hydrogenation to methanol

Hasliza Bahruji [a], Michael Bowker [a,b,*], Graham Hutchings [a], Nikolaos Dimitratos [a], Peter Wells [b,c], Emma Gibson [b,c], Wilm Jones [a,b], Catherine Brookes [a,b], David Morgan [a], Georgi Lalev [a]

[a] Cardiff Catalysis Institute, School of Chemistry, Cardiff University, Main Building, Park Place, CF10 3AT Cardiff, UK
[b] The UK Catalysis Hub, Research Complex at Harwell, Harwell, Oxon OX11 0FA, UK
[c] Department of Chemistry, University College London, Gordon Street, London WC1H 0AJ, UK

ARTICLE INFO

Article history:
Received 28 October 2015
Revised 15 January 2016
Accepted 15 March 2016
Available online 1 April 2016

Keywords:
Methanol synthesis
CO_2 hydrogenation
Pd/ZnO
PdZn alloy
Sol immobilisation

ABSTRACT

The direct hydrogenation of CO_2 into methanol is crucial for providing a means of CO_2 fixation and a way to store cleanly produced hydrogen in a more energy-dense and transportable form. Here we have prepared two series of Pd/ZnO catalysts, both by immobilisation of PVA-protected Pd colloids and by Pd impregnation of $PdCl_2$ to investigate structure activity relationships for direct CO_2 hydrogenation. Very different performances were found for the different preparation methods, and the Pd loading and pre-reduction of the catalysts were shown to be important factors for optimising methanol yield. The crucial factor for high methanol yield is the formation of a Pd–Zn alloy, either during the reaction itself, or better by high temperature pre-reduction. The formation of the alloy greatly reduces CO production by the reverse water gas shift reaction. The catalysts prepared by sol-immobilisation were relatively stable to thermal treatment. In contrast, the impregnated catalysts were much less thermally stable, due to the presence of remnant chloride on the surface of the catalyst, which was absent for the case of sol immobilisation preparation. The results illustrate the importance of controlling the PdZn particle size and its surface structure for the catalysts to achieve high methanol selectivity (60%, the rest being CO) and conversion (11%) at 250 °C and 20 bar. Selectivity for sol-immobilised catalysts decreases from 60% at 3 nm average diameter, to 20% at 7 nm.

1. Introduction

Methanol is one of the top ten industrial commodities with annual consumption of 53 million tonnes in 2011 [1] and is currently produced from synthesis gas, a mixture of CO_2, CO and H_2 derived from natural gas. The reaction takes place in industry over $Cu/ZnO/Al_2O_3$ catalysts with reaction conditions of 50 bar pressure and a temperature of 250 °C [2]. There is a growing interest in producing a more sustainable route to methanol, that is, avoiding the use of fossil fuels, both as a commodity chemical in its own right, but also as a transportable form of hydrogen which itself is produced from solar energy [3]. It is feasible to produce methanol kinetically with CO_2 as the carbon source for methanol synthesis, providing a renewable or sustainable source of H_2 is available. This was shown by early work at the company which developed the current industrial catalyst (ICI) [4]. CO is present in the industrial process to reduce self poisoning by adsorbed oxygen, and hence increases rates. Also, CO_2 hydrogenation to methanol is thermodynamically an exergonic process. It is favoured at low temperature and high pressure conditions. However, methanol production is in competition with CO formation via the reverse water gas shift reaction (RWGS), and with C–O bond dissociation and hydrogenation reactions such as methanation [5].

Research to date has been focused on finding selective catalysts that can activate CO_2 under mild reaction conditions with high selectivity towards methanol. Cu based catalysts are reported to have high activity towards methanol production [6]. The underlying mechanism is not fully understood, however Cu was suggested to be the location for adsorbing CO_2, whilst Zn provided active sites for H_2 adsorption [7]. Maintaining the Cu^o oxidation state is also crucially important [8]. More recently, workers have returned to an old theme in methanol catalysis – namely the formation of a Cu–Zn alloy as the active phase in synthesis [9]. Nakamura et al. consider that the alloy interface is the active phase in CO_2 hydrogenation to methanol [10]. Behrens et al. proposed that this surface alloy is rather specific, with Zn decorating steps at the Cu nanoparticle surface [11,12] and Kuld et al. [13] also think that the surface alloy is important for dictating selectivity to methanol, but indicate a very high level of Zn in the surface. A brief review of the current

* Corresponding author at: Cardiff Catalysis Institute, School of Chemistry, Cardiff University, Main Building, Park Place, CF10 3AT Cardiff, UK.

http://dx.doi.org/10.1016/j.jcat.2016.03.017
0021-9517/

state of the art for CO_2 hydrogenation to methanol is given by Behrens [14]. Properly tuning the interface is reported to have substantial benefits for methanol synthesis, reducing the apparent activation energy of the reaction. Studt et al. discovered Ni–Ga catalyst reduced CO_2 to methanol at ambient temperature with considerably lower CO production [15]. In contrast to Cu–Zn catalysts where both methanol and CO production occur on the same site, in Ni–Ga systems, the Ga-rich sites activate methanol formation; meanwhile, the nickel-rich sites facilitate CO synthesis. The work of Graciani et al. on Cu/CeO catalyst reports that the active site for methanol synthesis lies at the ceria–Cu interface [16]. Catalyst deactivation is a challenging aspect in methanol synthesis. Prieto et al. suggested by achieving optimum inter-particle spacing combined with a uniform distribution, Cu/silica catalysts exhibit a remarkable enhancement in stability compared to the commercial $Cu/ZnO/Al_2O_3$ [17]. Pd was reported as a promoter in Cu/ZnO catalysts for methanol synthesis by maintaining the reduced state of Cu via hydrogen spillover from Pd to Cu [18]. Pd is also active for CO_2 hydrogenation and the resulting products depend on the type of support and the promoter [19]. Table 1 lists the studies on Pd catalysts with several metal oxide supports and additives for methanol synthesis. Various metal oxide supports have been used, leading to the formation of different Pd-based active species during the CO_2 hydrogenation reaction. In 2012 Collins et al. reported that a Pd–Ga bimetallic phase was formed in $Pd/Ga/Ga_2O_3$ catalysts which provides atomic hydrogen via spillover to the Ga_2O_3 surface which hampers both CH_3OH decomposition and CO production [20]. In addition, the high activity in Pd/Ga_2O_3 is ascribed to the optimal amount of Pd^{n+} ($0 < n < 2$) species stabilised by Ga_xO_y suboxide layer on the surface of Pd [21]. Reductive formation of Pd2Ga nanoparticles was also reported by Ota et al. for catalysts made from substituted hydrotalcite-like precursors [22]. Koizumi and co-workers have investigated the effect of mesoporous silica supports and alkali promoters on the activity of Pd catalysts. Whilst the mesoporous structure of the support ensures formation of small Pd^0 nanoparticles, Ca, Mg and K promoters were essential to increase methanol yield [23]. Multi-walled carbon nanotube-supported Pd/ZnO catalyst was reported to reversibly adsorb large amount of hydrogen on the surface. This characteristic generates a micro-environment with higher concentration of active H-adspecies at the surface of the functioning catalyst, thus increasing the rate of surface hydrogenation reactions [24].

Pd/ZnO is active for oxidising methanol to CO_2 and H_2 and such activity emerges as a result of the formation of a Pd–Zn bimetallic structure [25,26]. The PdZn alloy formed on reduction of Pd–ZnO is responsible for high selectivity towards CO_2 production. PdZn based catalyst possesses long term stability for methanol steam reforming compared to $Cu/Zn/Al_2O_3$ commercial BASF catalyst [27]. The PdZn binary phase changes with the reduction temperature; the β-PdZn (1:1) alloy first forms at 200 °C, but further reduction at higher temperature produced a Zn rich β-PdZn alloy [28]. Stability studies of Pd–Zn alloys show loss of Zn at 550 °C to produce the Pd_2Zn binary phase [28]. Hydrogen spillover on Pd surfaces results in reduction of ZnO around the Pd periphery, forming a PdZn alloy. There are, however, different reports on the influence of PdZn alloys towards CO_2 hydrogenation. Kim and co-workers suggested that a Pd–Zn bimetallic species leads to deactivation of catalysts for methanol synthesis [29]. Liang and co-workers, however, proposed that the active site that was strongly associated with methanol formation was a Pd–Zn alloy rather than metallic Pd [24]. As can

Table 1
Catalytic properties of catalysts for CO_2 hydrogenation.

Catalysts	Reaction cond	System	Products	CO_2 Conv. (C) and CH_3OH Selectivity (S)	Ref.
Cu/SiO_2	4 MPa	Stainless steel reactor	CH_3OH	C: 15–20%	[17]
Impregnation	533 K			S: 98%	
$Ni/Ga/SiO_2$	0.1 MPa	Tubular fixed-bed reactor	CH_3OH	CH_3OH yield:	[15]
Impregnation	473 K		CO	0.25 $mol/mol_{activemetal}$ h	
PdZn	3 MPa	Stainless steel fixed-bed	CH_3OH	C: 0.6%	[22]
Co-precipitation	523 K	flow reactor	CO	S: 60%	
PdGa				C: 1%	
Co-precipitation				S: 47%	
Cu/CeO	CO_2: 0.05 MPa;	Fixed-bed reactor	CH_3OH	$TOF_{methanol}$: 1.3 mol/cm^2 s	[16]
	H_2: 0.45 MPa		CO		
	575 K				
$Cu/ZnO/Al_2O_3$ Co-precipitation	360 bar	Microreactor	CH_3OH	C: 37%	[30]
	533 K	$1CO_2$: $3H_2$	CO	S: 72%	
		$1CO_2$: $10H_2$	CH_3OH	C: 95% S: 98%	
			CO		
$Ga/Pd/β\text{-}Ga_2O_3$ impregnation Pd(Ac)	3 MPa	Plug flow reactor	CH_3OH, CO, DME	C: <1%	[20]
	523 K	$H_2/CO_2 = 3$		S: 52%	
Pd/Ga_2O_3	5 MPa	Flow reactor	CH_4, CO, $HCOOCH_3$,	C: 19.6	[21]
Co-precipitation $Pd(NO_3)_2$	523 K	$H_2/CO_2 = 3$	CH_3OH	S: 10.1	
Pd/ZnO	5 MPa	Flow reactor	CO, CH_3OH	C: 13.8	[21]
CO-precip $Pd(NO_3)_2$	523 K	$H_2/CO_2 = 3$		S: 37.5	
Pd/K/SBA-15 impregnation $Pd(NO_3)_2$	4.1 MPa	High-pressure fixed bed reactor	CH_3OH	C: 13	[23]
	523 K		CO	S: 11	
Pd/ZnO impregnation $Pd(NO_3)_2$	3.9 MPa	Conventional	CH_3OH	C: 11.4	[29]
	523 K	Flow high-pressure	CO	S: 50	
Pd/ZnO	3.9 MPa	Conventional	CH_3OH	C: 11.2	[29]
Deposi-co-preci $Pd(NO_3)_2$	523 K	Flow high-pressure	CO	S: 50	
Pd/ZnO/CNT Impregnation $PdCl_2$	3.0 MPa	Conventional fixed-bed flow reactor.	CH_3OH	C: 7.58	[24]
	523 K		CO	S: 95	
$Cu/Zn/Ga/SiO_2$ Co-impregnation	2 MPa	Fixed-bed continuous flow	CH_3OH	C: 5.6	[31]
	523 K		CO	S: 99.5	
$Cu/Ga_2O_3/ZrO_2$ deposition precipitation	2MPA	Fixed-bed continuous flow	CH_3OH	C: 13.71	[32]
	523 K		CO	S: 75.59	
$Cu/Zn/Al/ZrO_2$ Co-precipitation	4 MPa	Fixed-bed reactor	CH_3OH	C: 18.7	[33]
	513 K		CO	S: 47.2	

be seen then, there is some confusion regarding the exact role of the phases present in these catalysts.

The present study focuses on controlling the form of the Pd nanoparticles deposited onto the ZnO support. We used two preparation methods, one an impregnation method and the second is based on the colloidal formation of preformed Pd nanoparticles and their immobilisation on the ZnO support. The advantage of the second method is the control of particle size of the Pd nanoparticles prior to the deposition and avoidance of the heat/reductive treatment to form metal nanoparticles. Comparison of the two methodologies provides information about the role of Pd in terms of the significance of particle size and oxidation state in the formation of the PdZn bimetallic phase. The catalytic performance of the Pd/ZnO catalysts is crucially dependent on these methods and on the resulting physical characteristics.

2. Experimental

2.1. Catalyst preparation

Catalysts were made with palladium loadings on ZnO of 1 wt% and 5 wt%. The catalysts were prepared using both incipient wetness impregnation and sol-immobilisation methods. For impregnation, 2 mL of $PdCl_2$ (Sigma Aldrich) acidic solution was added onto 2 g of ZnO (Sigma Aldrich) powder and mixed thoroughly until it formed a paste. The paste was then dried in static air (120 °C, 2 h) followed by reduction in flowing H_2 at 400 °C for 3 h. This produced a 1% loading and for higher Pd wt% this step was repeated several times to reach the desired loading. For sol-immobilised catalysts polyvinyl alcohol was used as the stabiliser and $NaBH_4$ as reducing agent. An aqueous solution of $PdCl_2$ (Johnson Matthey) of the desired concentration was prepared. Polyvinyl alcohol (PVA, 1 wt% solution, Aldrich, Mw = 10,000, 80% hydrolysed) was added (PVA/Pd = 1.2 weight ratio). A 0.1 M freshly prepared solution of $NaBH_4$ (>96% Aldrich, $NaBH_4$/Pd = 5 molar ratio) was then added to form a dark-brown sol. After 30 min of sol generation, the colloid was immobilised by adding ZnO (acidified at pH 1 by sulphuric acid) under vigorous stirring conditions. The amount of support required was calculated to give the loadings of 1 and 5 wt%. After 2 h the slurry was filtered and washed with deionised water before drying in air (120 °C, 16 h). In what follows, IM denotes impregnation catalysts and SI denotes sol-immobilisation catalysts.

2.2. Catalyst characterisation

The characterisation of the samples was performed using a range of techniques. Powder X-ray diffraction (PXRD) patterns were obtained at room temperature with an Enraf Nonus FR590 diffractometer fitted with a hemispherical analyzer, using Cu Kα radiation (λ = 1.54 Å). X-ray photoelectron spectra (XPS) were recorded on a Kratos Axis Ultra-DLD XPS spectrometer with a monochromatic Al kα source (75–150 W) and analyser pass energies of 160 eV (for survey scans) or 40 eV (for detailed scans). Samples were mounted using a double-sided adhesive tape and binding energies referenced to the C (1s) binding energy of adventitious carbon contamination which was taken to be 284.7 eV. Data were analysed using Casa XPS software [34].

Pd K edge X-ray absorption spectra (XAS) were obtained on the B18 beamline at Diamond Light Source, Harwell, UK. Measurements were performed using a QEXAFS set-up with a fast-scanning Si (311) double crystal monochromator. The time resolution of the spectra reported herein was 1 min/spectrum (k_{max} = 16, step size 0.5 eV), and on average six scans were acquired to improve the signal to noise level of the data for transmission measurements. All samples were diluted with cellulose and pressed into pellets to optimise the effective edge-step of the X-ray absorption fine structure (XAFS) data and measured in transmission mode using ion chamber detectors. All XAFS spectra were acquired concurrently with the appropriate foil placed between I_t and I_{ref}. XAFS data processing was performed using IFEFFIT [35] with the Horae package [36] (Athena and Artemis). The amplitude reduction factor, S_0^2, was derived from EXAFS data analysis of a known reference materials and used as a fixed input parameter.

To provide detailed morphological and compositional information about the studied samples at micro and nano-scale, high-resolution transmission electron microscope (HRTEM) system JEOL 2100 (LaB6) is employed. For the analysis, the material was ground and mixed with water and 2 mL of materials in water suspension was placed on the TEM grid and dried. The instrument is equipped with a high-resolution Gatan digital camera (2 k × 2 k) with a maximum resolution of 0.2 Å giving us the ability to see crystal lattices, to obtain diffraction patterns and giving accurate measurement of the lattice d spacing utilising Digital Micrograph software. In scanning transmission electron microscopy (STEM) mode, dark field (HAADF/Z-contrast) detector was used to provide excellent compositional contrast. An energy dispersive X-ray spectrometer (EDS) system (Oxford Instruments), was equipped with a large-area 80 mm^2 SDD (Silicon Drift Detector). X-MaxN 80 T was employed for the elemental analysis in line scans, and elemental mapping modes. To analyse the EDS data, the latest version of AZtecTEM software was utilised.

2.3. Methanol synthesis

The catalytic performance of the Pd/ZnO catalysts for CO_2 hydrogenation was determined in a fixed-bed continuous-flow reactor. A catalyst (0.5 g) was placed in a stainless tube reactor with i.d. of 0.5 cm and length 50 cm with the catalysts packed in the middle of the tube, occupying ~10 cm. Prior to the reaction, catalysts were pre-reduced in a flow of 5% H_2/Ar gas (30 mL/min) for 1 h at 400 °C under atmospheric pressure. The reactor was cooled to 250 °C and a mixture of CO_2 and H_2 gases (1 CO_2: 3 H_2 molar ratios) was introduced with a flow rate of 30 mL min^{-1}. The pressure was increased to 20 bar using a back-pressure valve. All the post-reactor lines and valves were heated at 130 °C to avoid product condensation. The gas products were analysed using gas chromatography with (Clarus 450). Methanol was analysed using an Elite WAX ETR column and FID detector. CO_2, H_2, and CO gases were analysed using Carboxen-1000 column with TCD detector. Reported values are given after 3 h of reaction under steady state unless otherwise stated.

3. Characterisation results

3.1. PXRD

3.1.1. Impregnation catalysts

Characterisation of the IM catalysts was carried out using PXRD as shown in Fig. 1a. Pd/ZnO with 5 wt% loading was dried at 120 °C in air before reduction in a hydrogen flow at several temperatures. Pd/ZnO dried in air at 120 °C showed the presence of two peaks of PdO at 35.5° (110) and 38.7° (112) [37]. The pattern was similar after reduction at 150 °C, but a very broad peak appeared at 39.8° suggesting the presence of some nanoparticulate metallic Pd. Further reduction of the catalyst at higher temperature showed the disappearance of the Pd and PdO peaks. Two new peaks appeared at 41.7° and 43.8° corresponding to the reflection of the (111) and (200) β-PdZn alloy crystal planes respectively. Indeed it may be that these peaks are already present in the broad peaks at 150 °C.

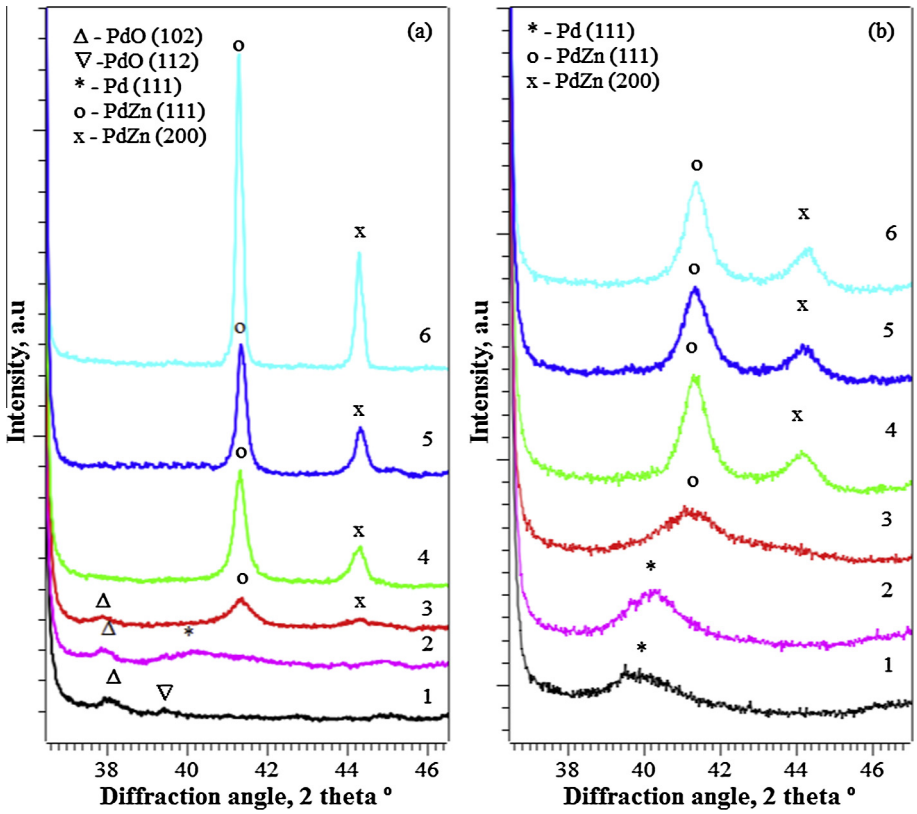

Fig. 1. PXRD patterns of 5 wt% Pd/ZnO catalysts prepared by impregnation (a) and sol immobilisation (b); (1) dried at 120 °C, (2) reduced at 150 °C, (3) at 250 °C, (4) at 400 °C, (5) at 550 °C and (6) at 700 °C.

3.1.2. Sol immobilisation catalysts

The PXRD patterns obtained for the synthesised sol-immobilised 5 wt% Pd/ZnO catalysts are given in Fig 1b. The dried 5 wt% Pd/ZnO catalyst showed a peak at 39.8° corresponding to the (1 1 1) reflection of Pd particles [38]. After reduction at 150 °C, the catalyst was still predominantly Pd although the peak slightly shifted to 40.1° and narrowed, due to an increase in the crystallite size of Pd. Reduction at 250 °C showed the presence of two new peaks appeared at 41.7° and 43.8° due to formation of the β-PdZn alloy. The formation of the β-PdZn alloy was accompanied by the disappearance of Pd particles indicating that the majority of Pd particles have incorporated Zn to form the β-PdZn alloy.

3.2. XPS analysis

3.2.1. Impregnation catalysts

The Pd (3d) XPS analysis of 5% Pd/ZnO prepared by the impregnation method is shown in Fig 2a. The Pd/ZnO fresh catalyst showed peaks at 336.5 eV and 341.8 eV, corresponding to PdO. However, there was clearly also chloride left in the catalysts, evidenced by the very high binding energy peak Pd peak at 338.4 eV, together with the Cl(2p) peak at 198.2 eV (Fig. S1 supplementary data). Reduction at 150 °C caused a shift of the main peak to a lower binding energy of 335.0 eV with a shoulder at 336.5 eV. This indicates the transformation of PdO into metallic Pd although there is still some PdO. Further reduction at 250 °C increased the intensity of the metallic Pd peak. Upon reduction at 400 °C, the PdO signal disappeared but still with the presence of a peak at 335.8 eV. XPS analysis also showed a significant level of chlorine on the surface of IM catalysts (Table 2). The chloride species was $PdCl_2$-like as evidenced by 337.8 eV signal and the presence of the Cl 2p peak at 198.3 eV (Fig. S2 supplementary data). The emergence of the peak at 335.8 eV indicates the formation of the PdZn alloy on the catalyst by reduction of the ZnO [39]. The alloying of Pd and Zn increases the binding energy of Pd (3d) levels and decreases the Zn (2p) levels. These shifts are caused by Pd (4d) → Zn (4p) charge transfer and a Pd (4d) → Pd (5 s, 5p) rehybridisation [40]. Further reduction to 400 °C and 550 °C increased the intensity of the PdZn peak and it appeared at the same binding energy of 335.8 eV. These results suggest that reduction between 400 °C and 700 °C only increases the crystallinity of PdZn alloy as we can observe from the PXRD patterns without varying the amount of Zn that is incorporated into the Pd lattice. XPS analysis also showed a significant level of chlorine on the surface and it was still present even after reduction at 700 °C.

3.2.2. Sol immobilisation catalysts

Fig. 2b shows the Pd (3d) XPS analysis of 5% Pd/ZnO prepared by sol immobilisation method after drying and reduction at 150 °C, 250 °C, 400 °C, 550 °C and 700 °C. Fresh catalysts showed the presence of Pd in the metallic state at 335.0 eV without the presence of PdO on the surface. This implies that the presence of the PVA ligand on the Pd surface protects the nanoparticles from air oxidation during exposure. Furthermore, the catalysts prepared by sol immobilisation show negligible amounts of chloride impurities on the surface, in contrast to the impregnation catalysts. After reduction at 150 °C the catalyst still exists as Pd metal, but after reduction at 250 °C there was a significant decrease in the intensity of the metallic Pd(3d) signal, with a shoulder arising at 335.9 eV due to alloying with Zn, which increased significantly when the reduction was carried out at 400 °C. Further reduction up to 700 °C showed little change in the features. We believe that during the catalytic reaction, the Pd exists as the PdZn alloy. Surface studies of a PdZn alloy on Ru showed that after reduction at 650 K, PdZn

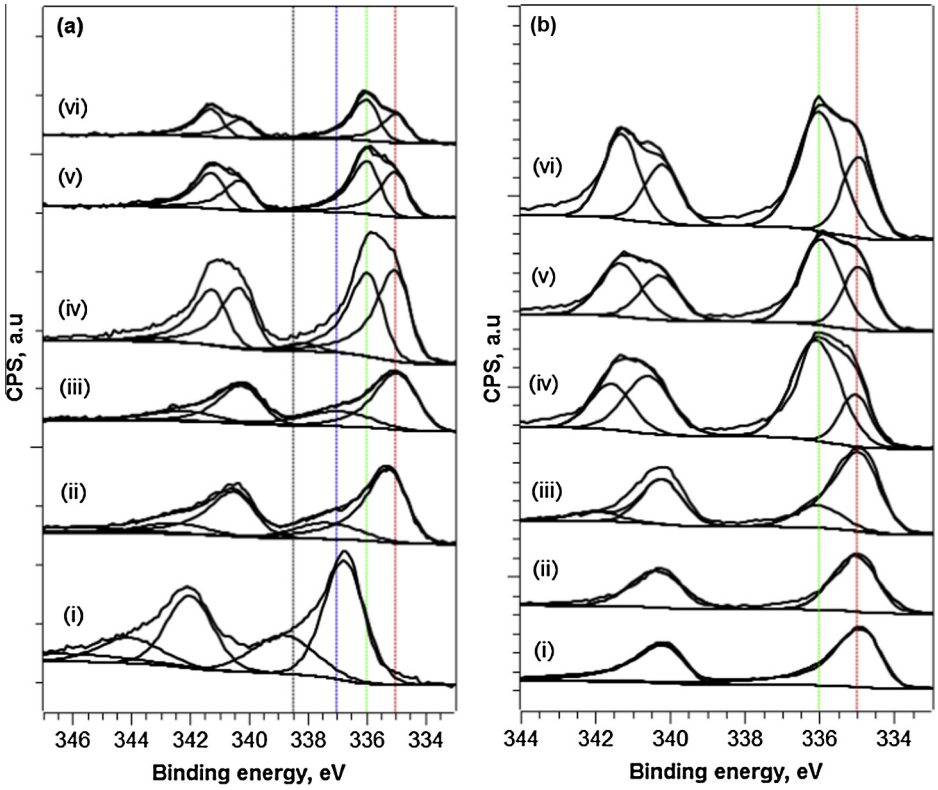

Fig. 2. Pd XPS spectra of 5% Pd–ZnO catalysts prepared by (a) the impregnation method and (b) the sol immobilisation method. The catalysts were dried at 120 °C (i), and reduced at 150 °C (ii), 250 °C (iii), 400 °C (iv), 550 °C (v) and 700 °C (vi). The red line is due to Pd metal at 335.0 eV, the blue line corresponds with the PdZn alloy at 336.0 eV, the green line is PdO at 337.0 eV and the black line is due to $PdCl_2$ at 338.4 eV.

Table 2
Particle size of Pd and PdZn supported on ZnO derived from TEM analysis. Also shown is the percentage of chlorine derived from XPS measurement.

Catalysts	Pre-treatment	Particle size, size (nm)	XPS derived Cl content (%)
5 wt% Pd ZnO IM	Air, 120 °C	1.4	4.3
	H_2, 150 °C	3.2	4.2
	H_2, 250 °C	6.3	4.6
	H_2, 400 °C	8.8	3.4
	H_2, 550 °C	9.3	4.6
	H_2, 700 °C	28.3	2.0
5 wt% Pd ZnO SI	Air, 120 °C	3.1	0
	H_2, 150 °C	2.8	0
	H_2, 250 °C	4.3	0
	H_2, 400 °C	4.9	0
	H_2, 550 °C	5.4	0
	H_2, 700 °C	7.3	0

was lost with Zn desorbing and Pd remaining on top of the support [40]; here, the system seems to be stable at elevated temperatures.

3.3. XAFS analysis

XAFS is a powerful technique for the study of nanoparticle systems as it is not reliant on long-range order to provide structural information and has been widely used to study Pd/ZnO systems [41–44]. EXAFS data of the Pd/ZnO catalysts were acquired to identify the nature of Pd within the samples at different stages of the treatment regime. The k^3 weighted χ and Fourier transform for the Pd/ZnO catalysts are shown in Figs. 3 and 4, respectively, along with the simulated fitting parameters in Table 3. The EXAFS data of the sol-immobilised catalyst dried in air at 120 °C and after reduction at 150 °C show that Pd is present as metallic nanoparticles with no evidence of alloying to Zn. The primary coordination environment can be modelled by a single Pd–Pd scattering path at 2.74 Å. The reduction in Pd–Pd coordination number, with respect to bulk Pd, from 12 to ~9 is indicative of nanoparticulate forms of Pd. Using the method developed by Beale and Weckhuysen [45] we can estimate that this corresponds to a particle size around 1.8 nm. The EXAFS data of the IM and SI Pd/ZnO systems reduced at 400 °C both show evidence of alloy formation. The main peak in the Fourier transform shifts to lower values of *R*, which corresponds to a Pd–Zn scattering path at 2.60 Å. This distance is indicative of Pd

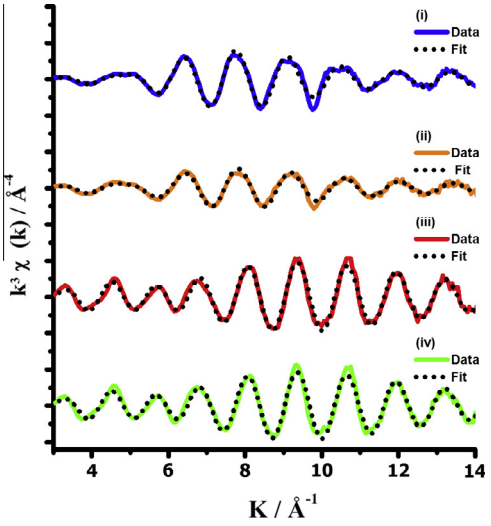

Fig. 3. K^3 weighted χ data for the Pd/ZnO catalysts: (i) IM and reduced at 400 °C, (ii) SI and reduced at 400 °C, (iii) SI and reduced at 150 °C, and the (iv) SI catalyst dried at 120 °C. For each sample the dashed black line represents the simulated fit.

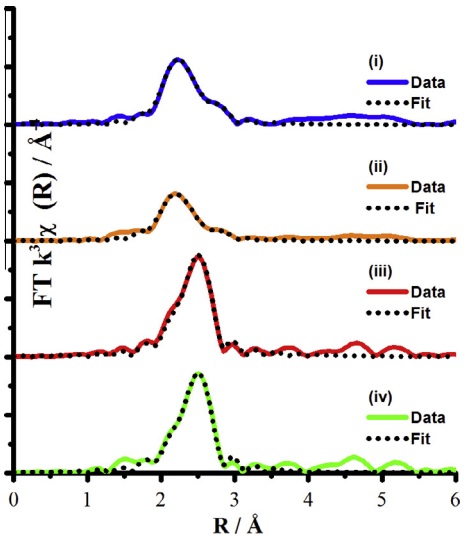

Fig. 4. K^3 weighted Fourier transform (magnitude) EXAFS data for the Pd/ZnO catalysts: (i) IM and reduced at 400 °C, (ii) SI and reduced at 400 °C, (iii) SI and reduced at 150 °C, and (iv) the SI catalyst dried at 120 °C. For each sample the dashed black line represents the simulated fit.

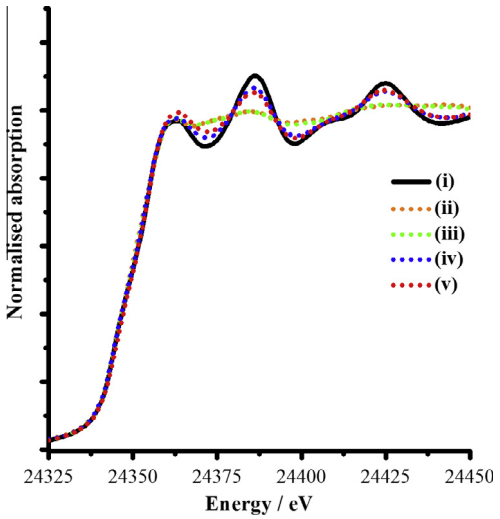

Fig. 5. Normalised XANES data for the Pd/ZnO catalysts: (i) Pd foil, (ii) IM and reduced at 400 °C, (iii) SI and reduced at 400 °C, (iv) SI and reduced at 150 °C, and (v) the SI catalyst dried at 120 °C.

alloyed with Zn and is accompanied by the associated Pd–Pd scattering path at 2.85 Å. However, to achieve a good level of fit another Pd–Pd path for non-alloyed Pd also needs to be included. This confirms that Pd is present as a PdZn alloy as well as some component with Pd only. The IM prepared catalyst reduced at 400 °C shows the most extensive alloying, with a greater coordination number for alloyed Pd–Zn and a reduced coordination number for the non-alloyed Pd–Pd distance. There is also a reduction in the non-alloyed Pd–Pd distance from 2.74 Å to 2.69 Å. A reduced M-M distance is consistent with a reduction in particle size or pseudomorphic overlayers and suggests that there may be some segregation within the PdZn NPs.

The XANES data of the Pd/ZnO samples (Fig. 5) support the EXAFS observations. The sol-immobilised Pd/ZnO systems dried at 120 °C and reduced at 150 °C are similar to the Pd foil, but with a reduction in amplitude of the XANES features because of a decreased particle size. The confirmation of PdZn alloy formation by differences in the XANES spectra has been reported previously [43,44] and is evidenced by decreases in the features at 24,390 eV and 24,430 eV and the appearance of a new feature at 24,400 eV. These changes are also observed for the IM and the SI Pd/ZnO systems reduced at 400 °C.

3.4. Nanostructural analysis by TEM

3.4.1. Impregnation catalysts

TEM was used to characterise the morphology of the catalysts, especially to acquire the PdZn particle size distribution after various reduction treatments. Representative TEM images of 5 wt % Pd/ZnO catalysts prepared by the impregnation method and the Pd particle size histograms of the catalysts are shown in Fig. 6. Large particles with average diameter of 11.3 ± 4 nm (Fig. 6a) were produced after calcination in air at 500 °C, and were in a similar size when the air-calcined catalyst was reduced at 400 °C (Fig. 6b). Catalysts synthesised by impregnation and calcination often produce large metal nanoparticles [46]. Calcination at 500 °C causes sintering of the small Pd particles formed at lower temperature to produce larger particles.

Fig. 7 shows representative TEM images and histograms of 5 wt % Pd/ZnO catalysts dried at 120 °C followed by heating treatment under a flow of H_2 gas at 150–700 °C without prior air calcination. The catalyst dried in air at 120 °C produced Pd nanoparticles with average particle size of 1.4 nm (Fig. 7a). Annealing the catalysts under H_2 flow formed more uniform particles, with relatively smaller particles than the catalysts that were calcined in air as expected. Larger aggregates of Pd particles were noticeable as the catalysts were reduced at high temperature and reduction at 700 °C increased the particle size to 25.3 nm (Fig. 7f).

3.4.2. Sol immobilisation catalysts

The TEM analysis of 5 wt% Pd/ZnO prepared by sol immobilisation method (Fig. 8) provides evidence that the Pd nanoparticles were evenly distributed on the ZnO support. The particle size distribution was calculated by measuring particle diameters in several images for Pd/ZnO catalysts. The as-prepared catalyst formed a uniformly distributed Pd particle with the average diameter of 3.1 nm (Fig. 8a). The particle size increased to

Table 3
EXAFS distances and fitting parameters for the Pd/ZnO catalysts.

Sample	Abs Sc	*N*	*R* (Å)	$2\sigma^2$ (Å^2)	E_f (eV)	R_{factor}
Pd/ZnO (SI, fresh)	Pd–Pd	9.1 (3)	2.738 (3)	0.007 (1)	3(1)	0.02
Pd/ZnO (SI, reduced at 150 °C)	Pd–Pd	9.2 (3)	2.738 (3)	0.007 (1)	4(1)	0.01
Pd/ZnO (SI, reduced at 400 °C)	Pd–Zn	4.5 (4)	2.60 (2)	0.007 (1)	1(2)	0.03
	Pd–Pd	2.0 (5)	2.67 (4)	0.009 (3)		
	Pd–Pd	2.5 (5)	2.85 (3)	0.010 (1)		
Pd/ZnO (IM, reduced at 400 °C)	Pd–Zn	6.4 (3)	2.62 (1)	0.007 (1)	4(2)	0.01
	Pd–Pd	1.5 (4)	2.69 (3)	0.007 (2)		
	Pd–Pd	3.4 (4)	2.88 (1)	0.008 (1)		

Fitting parameters: $S_0^2 = 0.8$ as deduced by Pd foil reference; Fit range $3 < k < 14$, $1 < R < 3.5$; # of independent points = 17.

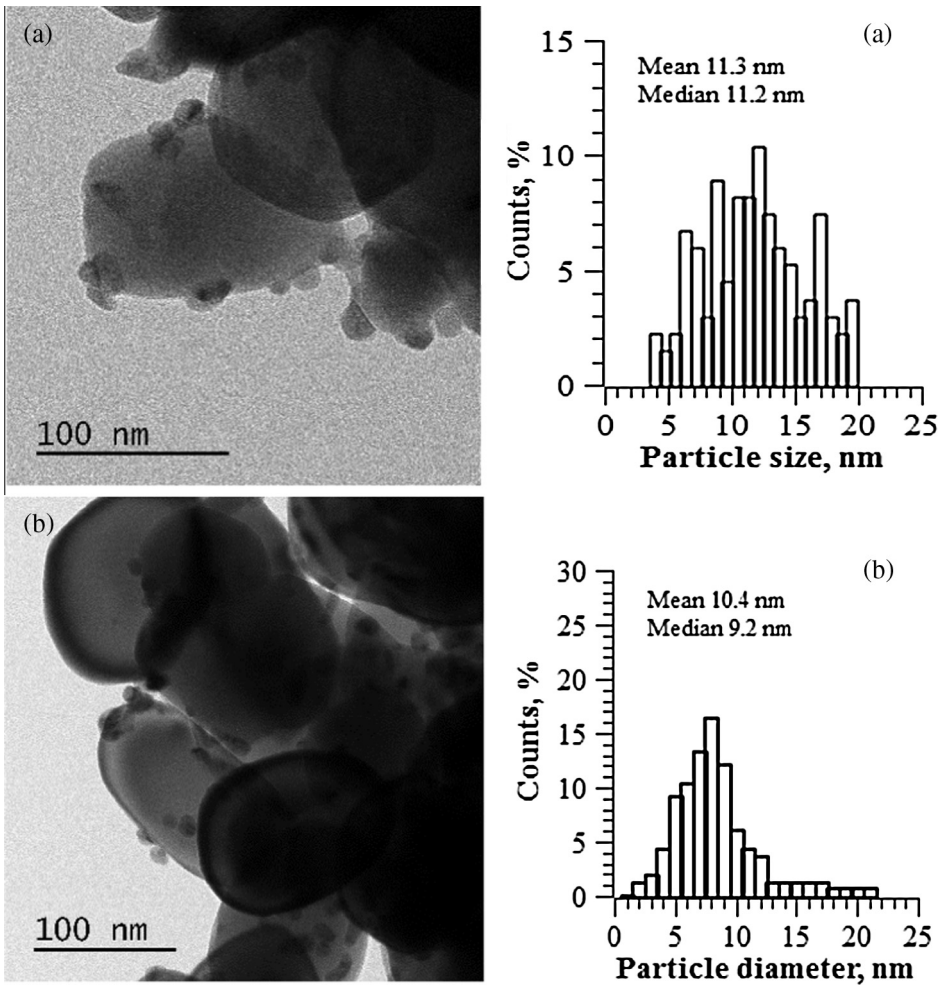

Fig. 6. Representative TEM images and the corresponding histograms of the Pd particle size distributions for 5% Pd/ZnO catalysts prepared by the impregnation method (a) catalysts calcined in air at 500 °C with mean Pd diameter of 11.3 ± 4 nm and (b) followed by reduction at 400 °C with mean Pd diameter of 10.4 ± 4 nm.

7.3 nm as the reduction temperature increased to 700 °C (Fig. 8f), showing greater size stability than the incipient wetness catalysts. Elemental mapping of the catalysts (supplementary Fig. S3) was carried out to confirm and measure the amount of Pd. The measured wt% of Pd was 5.6 on the catalyst implying that preformed Pd nanoparticles, stabilised by PVA, have been well deposited onto the ZnO support.

4. Methanol synthesis

4.1. Comparing Pd/ZnO catalysts from impregnation and sol immobilisation methods

The activity of the catalysts was evaluated for the CO_2 hydrogenation reaction and the major products were methanol and CO. The reaction was carried out at 250 °C and 20 bar pressure. Catalysts were reduced in H_2 at 400 °C prior to the reaction to ensure that the PdZn species was formed. Analysis of the gaseous products confirms the production of methanol and carbon monoxide, and no methane was observed.

Fig. 9a shows the time dependence of activity/selectivity of 5% Pd/ZnO IM catalyst. The presence of CO with ~99% selectivity at 12% of CO_2 conversion shows that RWGS dominates the reaction. The catalyst also shows some deactivation over reaction time and the conversion stabilises at 8% after 60 min and maintains this value for the measuring period of 4 h.

In contrast, the 5 wt% Pd/ZnO made by sol immobilisation showed a very different activity. The reaction (Fig. 9b) started with high selectivity of methanol (70%) and experienced a slight deactivation. It reached steady state after 3 h reaction with 60% selectivity of methanol at 10.7% conversion.

The effect of Pd loading was studied at 1 and 5 wt%. The results summarised in Table 4 were obtained after 3 h of reaction, when the reaction had reached a steady state. As loading increases, so does conversion, though methanol selectivity diminishes somewhat for the highest loading. The IM catalysts show worse selectivity than the SI ones.

In addition, we have also investigated the effect of calcination temperature on the 5 wt% Pd/ZnO sol immobilised catalysts, Table 5. The catalytic activity is similar at all calcination temperatures, except 700 °C where there is some loss of activity. There is a slight diminishment of selectivity for the SI catalyst by 500 °C, but CO dominates the products after high temperature calcination.

It is important to study the effect of reduction temperature in the performance of the catalyst, since that is related to the PdZn formation. The 5 wt% Pd/ZnO IM catalyst was dried at 120 °C before being treated under pure H_2 at 150 °C, 250 °C, 400 °C, 550 °C and 700 °C. No catalytic activity was observed on the catalyst that was reduced at 150 °C. An increase in activity was observed when catalysts were reduced from 250 °C to 550 °C (Table 6). After reduction at 550 °C CO_2 conversion was at 9% and CO was the only product. Further reduction at 700 °C had a detrimental effect on catalytic activity with 0.7% CO_2 conversion, indicating deactivation of the catalyst.

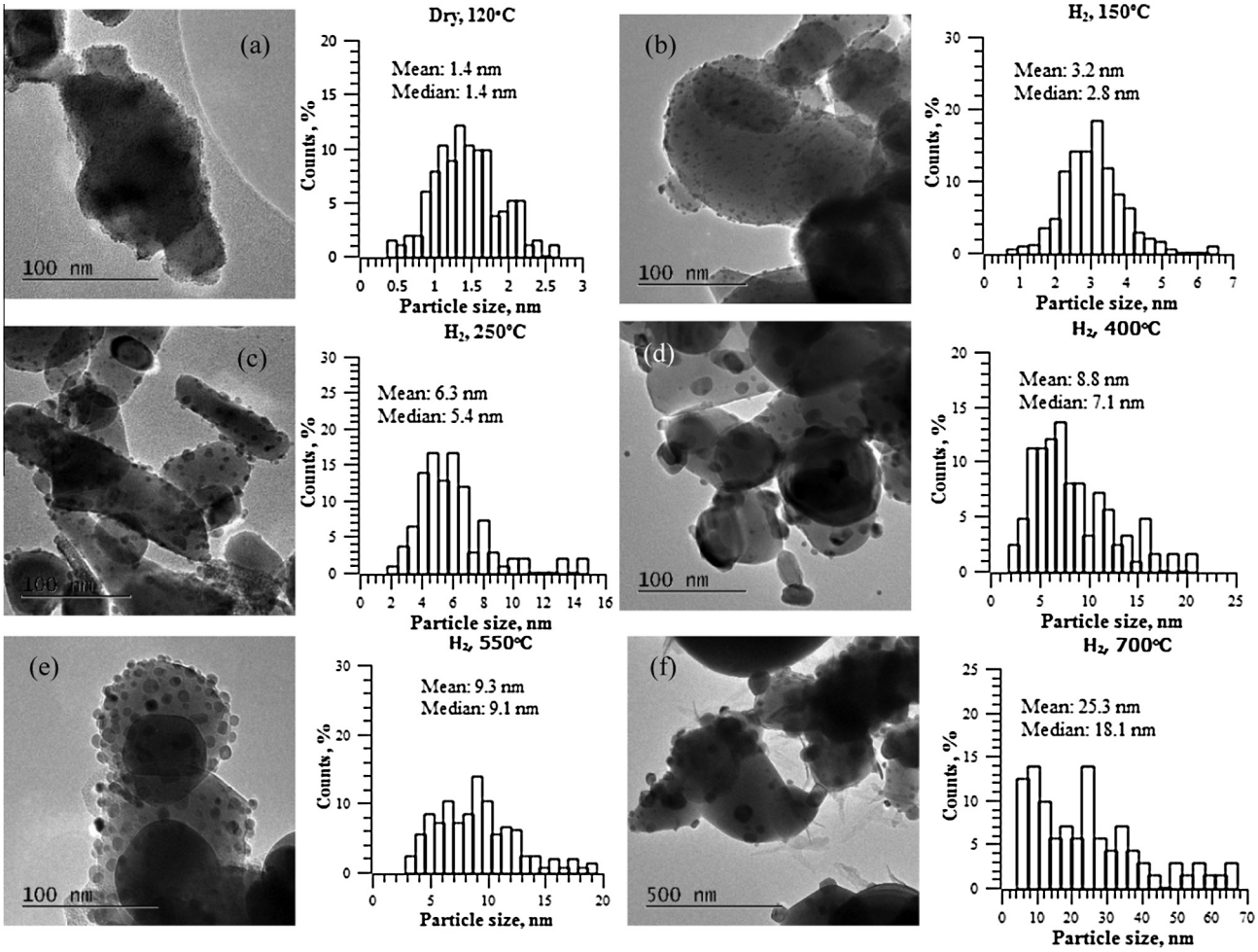

Fig. 7. TEM images and the corresponding histograms of the Pd particle size distributions for 5% Pd/ZnO catalysts prepared by the impregnation method without air calcination (a) catalyst dried at 120 °C, and after heating in H_2 at (b) 150 °C, (c) 250 °C, (d) 400 °C, (e) 550 °C and (f) 700 °C.

For the SI catalyst the CO_2 conversion significantly increased for reduction up to 400 °C, but then decreased at higher pre-reduction temperatures, down to 5.6% at 700 °C. On the other hand, methanol selectivity change increased with the temperature being 72% at the highest pre-reduction temperature. Significant improvement on the rate of CH_3OH formation was observed after reduction at 400 °C with methanol produced at the highest rate of 2423 mmol kg_{cat}^{-1} h^{-1}. It is interesting to note that annealing the catalysts in H_2 at 700 °C only gives a relatively small deactivation with the CH_3OH rate at 1400 mmol kg_{cat}^{-1} h^{-1}

4.2. The influence of the Pd and PdZn bimetallic phase on CO_2 hydrogenation reaction on sol immobilised catalysts

In order to further investigate the influence of the PdZn bimetallic phase on the catalyst activity, the reaction temperature varied from 150 to 300 °C using the 5 wt% Pd ZnO sol immobilised catalyst. The catalyst was reduced in H_2 at 150 °C and 400 °C for 2 h to form, respectively the Pd and PdZn phases on the ZnO support. XPS and PXRD analyses of the catalyst reduced at 150 °C confirm the Pd is still present as Pd metal. The catalyst reduced at 150 °C, Fig 10a, shows 10% CO_2 conversion at 150 °C reaction temperature, with 98% selectivity of CO. The conversion reduced to 8% when the temperature was increased to 200 °C with a significant production of methanol at ~20% selectivity. Methanol production increased continuously as the reaction temperature was increased to 275 °C. The formation of the PdZn phase presumably takes place in situ during the reaction, beginning at ~180 °C, where the change in selectivity profile begins, and consequently is the cause of improved CH_3OH formation.

PXRD and XPS analyses confirmed the formation of a β-PdZn alloy when the 5 wt% Pd/ZnO SI was reduced at 400 °C. At 150 °C, as shown in Fig. 10b, there is a very low conversion of CO_2 at ~1%. CH_3OH was produced as the main product with only a trace of CO formed. The CO_2 conversion increased to 13% as the temperature was increased to 300 °C. The selectivity to methanol, however, continually decreased from 92% to 31%, but compared favourably with the selectivities seen for Pd–ZnO catalysts prepared more conventionally (Table 1). These observations provide clear evidence of the PdZn role in CO_2 hydrogenation reaction. Apart from favouring CH_3OH formation, PdZn also inhibits CO formation which occurs on the pure Pd surface, and there is a clear difference between the low temperature pre-reduction (giving Pd nanoparticles), and high temperature pre-reduction which produces Pd–Zn. The increase in CO formation at high reaction temperature is due to the thermodynamic limitation of the reaction, which favours the RWGS reaction as shown in Table 7 [47].

4.2.1. CO DRIFTS analysis of Pd/ZnO catalysts

DRIFTS was used to follow the adsorption of CO on the reduced IM and SI catalysts to provide insight into their structure. The samples had been previously reduced at 400 °C, before being transferred to the DRIFTS cell. CO adsorption was also performed on the SI sample after a mild in situ reduction in the DRIFTS cell under

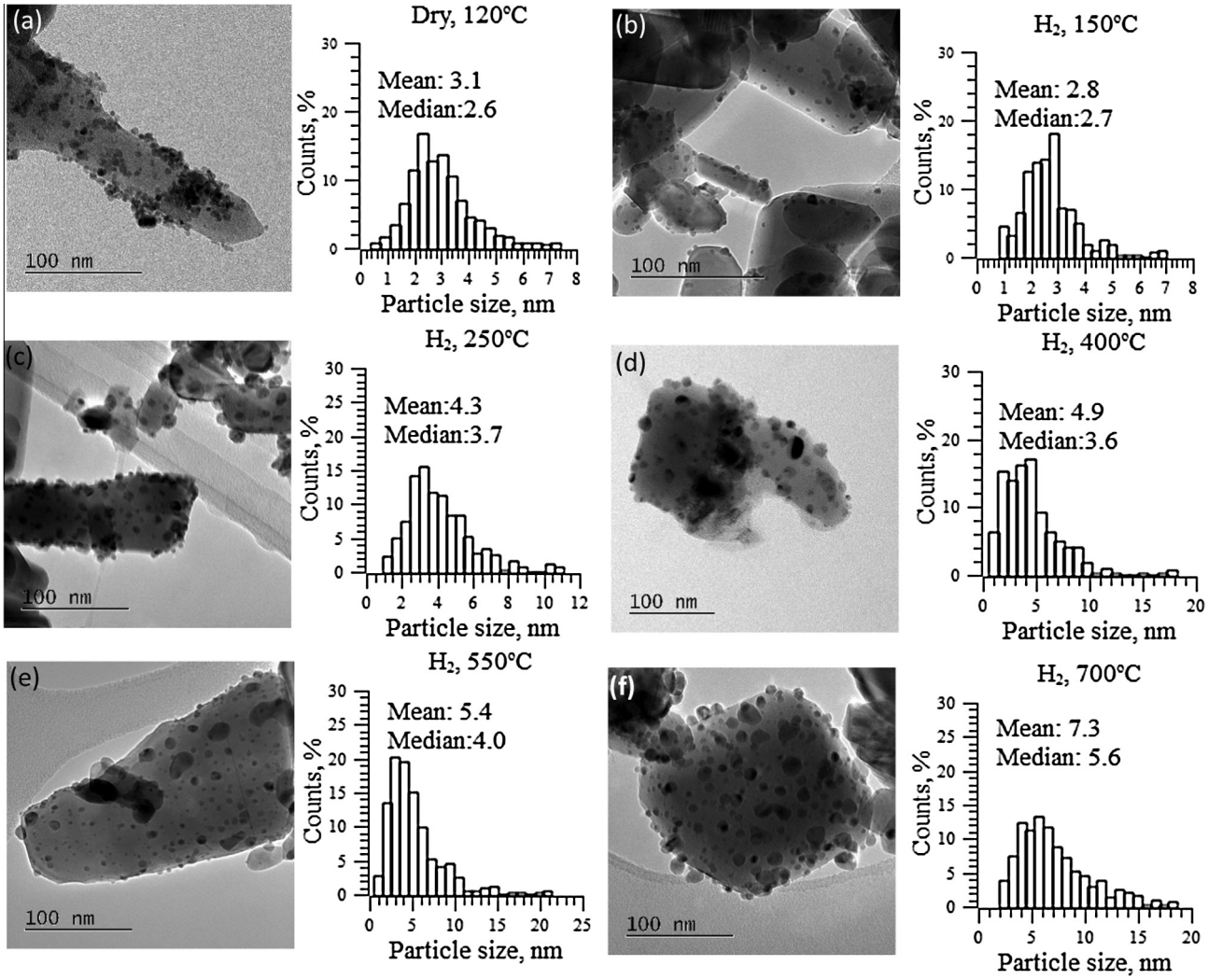

Fig. 8. Representative TEM images and the corresponding histograms of the Pd particle size distributions for 5% Pd/ZnO catalysts prepared by sol immobilisation method (a) catalyst dried at 120 °C, and after annealing in H_2 at (b) 150 °C, (c) 250 °C, (d) 400 °C, (e) 550 °C and (f) 700 °C.

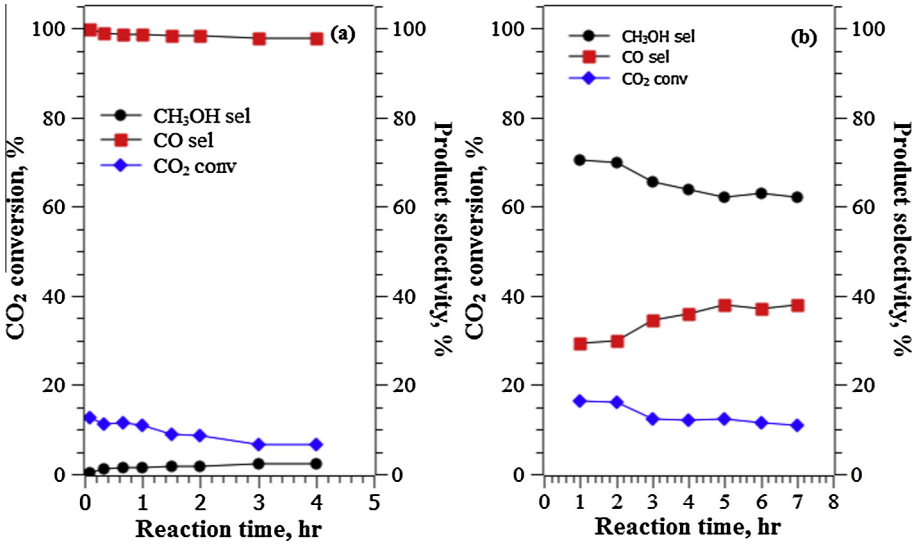

Fig. 9. CO_2 hydrogenation reaction on (a) 5% Pd/ZnO by impregnation and (b) 5% Pd/ZnO catalyst prepared by sol immobilisation method. The catalysts were pre-reduced prior to the reaction at 400 °C under flow of H_2. The reaction was carried out at 250 °C at 20 bar with $1CO_2$: $3H_2$ at 30 ml/min.

Table 4
CO_2 hydrogenation reaction on Pd/ZnO catalysts at various Pd loadings prepared using impregnation, IM and sol immobilisation, SI methods.

Catalysts	Conv. of CO_2 (%)	Selec. of CH_3OH (%)	Selec. of CO (%)	CH_3OH rate (mmol kg_{cat}^{-1} h^{-1})	CO rate (mmol kg_{cat}^{-1} h^{-1})
1% Pd, SI	1.7	76	24	410	150
1% Pd, IM	3.2	22	78	270	950
5% Pd, SI	10.7	60	39	2420	1050
5% Pd, IM	8.7	1	99	55	2970

Reaction conditions: 0.5 g catalyst, 30 ml/min 1 CO_2: 3 H_2 mixture, 20 bar, 250 °C. Catalytic activity was measured after 3 h reaction. All catalysts were pre-treated in situ at 400 °C with H_2 flow for 60 min.

H_2 at 150 °C. The spectra obtained for the three samples are shown in Fig. 11. Bands consistent with linearly adsorbed CO on Pd, bridge bonded CO on Pd and possibly CO adsorbed on PdO were observed at 2090 and 2067, 1980 and 1950 and 2125 cm^{-1} respectively on the SI catalyst post 400 °C reduction [48,49]. The linear CO band observed at 2081 cm^{-1} can be attributed to corner sites whereas the shoulder at 2067 cm^{-1} is a little high in wave number to be assigned to edge sites which are expected near 2050 cm^{-1} [50]. In comparison with the linear CO bands, the bridged CO features at 1980 and 1950 cm^{-1} are intense, implying the catalyst surface consisting of metallic Pd. The IM catalyst shows no linear CO bands but only bridged CO species.

The SI catalyst was reduced in situ in the DRIFTS cell and then CO adsorption was repeated. A significant reduction in the bridged CO feature relative to the linear CO band is observed compared to the ratio of these species for the externally reduced SI catalyst, Fig. 11(a and b). The linear CO band is observed at 2064 cm^{-1} and the linear CO species adsorbed on Pd corner atoms previously observed at 2081 cm^{-1} has disappeared. As XPS and XAFS results both show that the alloy phase has been formed for the SI sample reduced at 400 °C, then the band at 2064 cm^{-1} observed as a shoulder in the externally reduced SI catalyst and observed clearly in the in situ reduced sample' is tentatively assigned to CO linearly adsorbed on the PdZn alloy phase. In fact, a similar shift in the linear CO band to lower wave numbers has previously been observed for the formation of a PdZn alloy phase [44,51]. From these results we can infer that the alloy phase is present but not fully exposed at the surface of the externally reduced SI catalyst. This could be due to segregation of Pd to the surface on exposure to air during transfer from the reduction chamber to the DRIFTS cell.

4.2.2. Temperature programmed desorption studies of methanol on Pd/ZnO catalyst

We used methanol desorption/decomposition as probe reaction in an attempt to gain further information about the nature of the Pd/ZnO catalyst. The catalyst was pre-reduced at 150 °C and 400 °C respectively before being dosed with methanol. Fig. 12a and b shows the temperature programmed desorption, TPD, from the IM and SI catalysts after in situ reduction at 150 °C. They show little obvious desorption, except from some water and hydrogen and a peak for the SI catalyst of CO at 270 °C. Reduction of the catalysts followed by methanol adsorption and TPD at 400 °C is shown for IM (Fig 12c) and SI catalysts (Fig 12d). There is little obvious C product desorption from the IM catalyst, but significantly, on the SI catalyst, H_2 and CO_2 desorbed coincidently at ~550 K, which is indicative of the presence of a formate species on the surface, which is the common source of both products in the TPD at this temperature. It has been proposed that the formate species is the pivotal intermediate involved in methanol synthesis [52,53] on Cu-based catalysts. This finding indicates that the surface of the catalyst is very much modified, since Pd itself decomposes formate species below room temperature [54,55], and it is possible that PdZn predominantly covers the surface and stabilises the formate. Note that in the seminal work relating to methanol synthesis on ZnO [47] CO_2 was shown to be pivotal to formate formation and methanol synthesis. The formate species, however, were not observed on IM catalysts, perhaps because of the much lower metal surface area.

5. Discussion

Addressing the origin of catalytic activity for methanol production is important for improved catalyst design that can enhance the catalyst activity thereby enabling optimum materials and conditions for the reaction to be identified. The active sites for CO_2 hydrogenation and the RWGS reaction are different, and change as the Pd is transformed into the PdZn bimetallic phase. This has already been reported for other related reactions such as methanol steam reforming by Karim et al. [26,56]. We have focused on the synthesis of Pd nanoparticles with controlled mean particle size by using the sol preparation method, which allowed us to maintain a small particle size and good methanol yield. A mild reduction treatment of the immobilised catalyst enhanced the methanol selectivity; however, increasing the mean particle size of PdZn alloy beyond 4 nm decreased the methanol yield significantly for both impregnated and immobilised catalysts (Fig. 13). It is interesting to see that impregnated 5% catalyst only shows activity towards RWGS reaction despite the fact that PdZn particles were formed. However, we also found that the impregnation catalysts still contain Cl impurities which are strongly held on the catalyst surface, even after annealing at 700 °C and have a significant effect on the growth and sintering of Pd and PdZn nanoparticles. The rel-

Table 5
CO_2 hydrogenation for 5 wt% Pd/ZnO sol immobilised catalysts subjected to a variety of calcination pretreatments.

Catalysts	Pre-treatment	Conv. CO_2 (%)	Selectivity CH_3OH (%)	Selectivity CO (%)	CH_3OH rate (mmol kg_{cat}^{-1} h^{-1})	CO rate (mmol kg_{cat}^{-1} h^{-1})
5% Pd/ZnO SI	120 °C, air	10.7	60	39	2423	1050
	250 °C, air	10.8	60	39	2370	1570
	400 °C, air	11.1	59	40	2470	1700
	500 °C, air	10.3	54	45	2090	1770
	700 °C, air	7.2	22	77	540	2150
5% Pd/ZnO IM	120 °C, air	8.7	2.17	97.8	52	2480
	500 °C, air	8.5	1	99	55	2970

Reaction conditions: 0.5 g catalyst, 30 ml/min 1 CO_2: 3 H_2 mixture, 20 bar, 250 °C. Catalytic activity was measured after 3 h reaction. All catalysts were pre-treated in situ at 400 °C with H_2 flow for 60 min.

Table 6
Comparison of activity of 5% Pd/ZnO prepared by impregnation and sol immobilisation treated at various reduction temperatures.

Catalyst	Treatment	CO_2 Conv (%)	Selectivity CH_3OH (%)	Selectivity CO (%)	CH_3OH rate (mmol kg_{cat}^{-1} h^{-1})	CO rate (mmol kg_{cat}^{-1} h^{-1})
5% Pd/ZnO IM	150 °C[a], H_2	0	0	0	0	0
	250 °C[b], H_2	4.5	0	100	0	1690
	400 °C, H_2	6.7	2	98	52	2480
	550 °C, H_2	9.5	0	100	0	3550
	700 °C, H_2	0.7	26	74	69	198
5% Pd/ZnO SI	150 °C[a], H_2	8.7	48	52	1900	2450
	250 °C[b], H_2	7.9	58	42	2100	1440
	400 °C, H_2	10.7	60	39	2423	1050
	550 °C, H_2	6.3	64	36	1700	829
	700 °C, H_2	5.6	72	28	1400	540

Reaction conditions: 0.5 g catalyst, 30 ml/min 1 CO_2: 3 H_2 mixture, 20 bar, 250 °C. Catalytic activity was measured after 3 hr of reaction. All catalysts were pre-treated in situ at 400 °C with H_2 flow for 60 min apart from (a) at 150 °C and (b) at 250 °C.

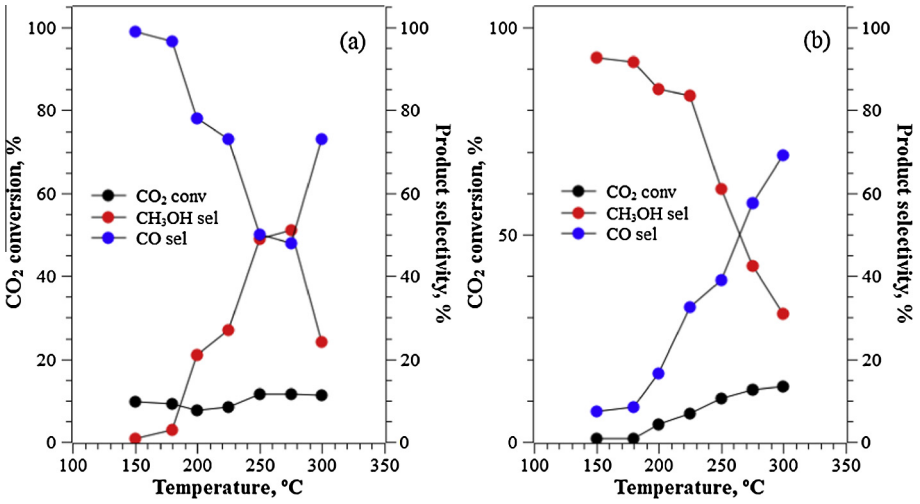

Fig. 10. CO_2 conversion, CH_3OH and CO selectivities as a function of reaction temperature (150–300 °C) on 5% Pd ZnO catalysts prepared by the sol immobilisation method. The catalyst was reduced at (a) 150 °C to form Pd/ZnO and (b) at 400 °C to form PdZn/ZnO catalyst.

Table 7
Summary of thermodynamic values of methanol synthesis and RWGS from CO_2.

Reaction	Temperature (°C)	ΔH^o (kJ mol^{-1})	ΔG^o (kJ mol^{-1})
$CO_2 + 3H_2 \rightarrow$ $CH_3OH_{(g)} + H_2O_{(g)}$	25	−49.5	+3.4
	225	−58.1	+41.5
$CO_2 + H_2 \rightarrow CO_{(g)} + H_2O_{(g)}$	25	+41.2	+28.6
	225	+39.8	+20.4

atively large PdZn particle size and the presence of chlorine contaminations are detrimental towards methanol selectivity, and it is likely that sintering is enhanced by the presence of chloride.

The two main types of reaction involved here are

(i) methanol production from CO_2 hydrogenation

$$CO_2 + 3H_2 \rightarrow CH_3OH + H_2O$$

(ii) CO production from the reverse water gas shift reaction.

$$CO_2 + H_2 \rightarrow CO + H_2O$$

There is also a possibility that some secondary methanol dehydrogenation occurs, but in turn the CO could contribute to produce CH_3OH. Pd is an effective methanol dissociation catalyst, breaking the C–H bond into CO and H_2. At low reaction temperature, supported Pd nanoparticles show high activity towards the reverse water gas shift reaction. We suggest that during the hydrogenation reaction, CO_2 adsorbs on ZnO to form carbonate-like surface complexes, as reported elsewhere [57–59]. CO_2 is unlikely to adsorb strongly on Pd [60] but Pd can easily dissociate H_2. Pd metal has a strong affinity towards CO and consequently formate intermediates on the oxide adjacent to the metal may undergo decomposi-

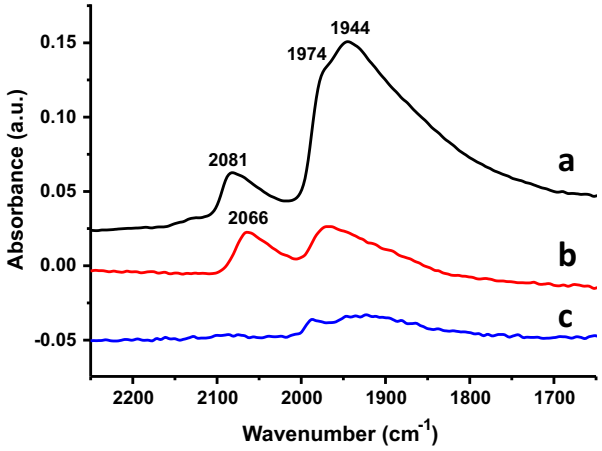

Fig. 11. DRIFTS spectra after purging with Helium for 10 min at RT after CO adsorption, (a) 5% Pd ZnO SI catalysts reduced at 400 °C, (b) 5% Pd ZnO SI reduced at 400 °C followed with in situ reduction at 150 °C and (c) 5% Pd ZnO IM reduced at 400 °C.

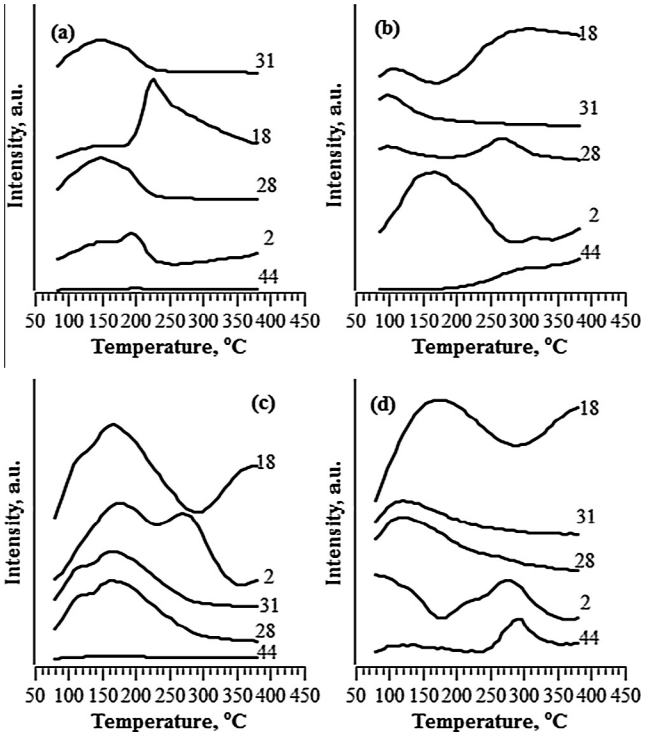

Fig. 12. Temperature programmed desorption after adsorption of methanol on 5% Pd/ZnO catalysts; (a) IM catalyst reduced at 150 °C; (b) SI catalyst reduced at 150 °C; (c) IM catalyst reduced at 400 °C; (d) IM catalyst reduced at 400 °C.

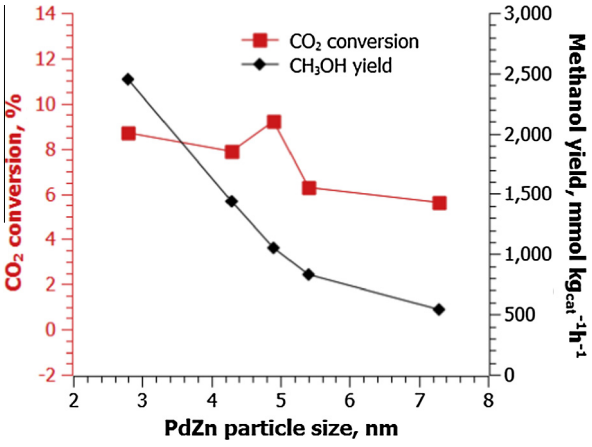

Fig. 13. CO_2 conversion and methanol production relationship with PdZn diameter for 5% Pd/ZnO prepared using sol immobilisation method. Reaction was carried out at 250 °C, 20 bar under the flow of 30 ml/min CO_2: $3H_2$. Catalytic activity was measured after 3 h reaction. All catalysts were pre-treated in situ at 400 °C with H_2 flow for 60 min.

tion on Pd. Further, formate intermediates, which have been shown to be pivotal intermediates for methanol synthesis [36] are very unstable on Pd metal and so will decompose there, rather than make methanol. Instead, it is probable that the formation of PdZn passivates the surface in this respect and stabilises the formate intermediate, as shown by the TPD result in Fig. 12, and so on to further hydrogenation to methanol. In effect the alloying converts the behaviour of Pd to be more like Cu. It has been shown that alloying Pd leads to charge transfer [61] to fill the d-band of Pd and thus shift it below the Fermi level – that is, more likely the group 11 metals. Reduction of the catalysts at high temperature may also contribute to an increase in oxygen vacancies on ZnO support. Oxygen vacancies on ZnO strengthen the CO_2 interaction by increasing the electron transfer to CO_2 from the polarons so-formed [62].

Ota et al. [22] compared alloys of Pd with Zn and with Ga, and found that both can make methanol, but selectivity is much better for the former. The intermetallic Pd_2Ga catalyst shows high performance as a hydrogenation catalyst, particularly for semi-hydrogenation reactions [63]. The activity of intermetallic PdGa is improved due by changes in electronic properties around the Fermi level in comparison with Pd metal [64]. Modifying the shape and surface properties of Ga_2O_3 enhances electron transfer to Pd metal at their Schottky-Mott interfaces which simultaneously improves catalytic performance [65].

Pd/ZnO prepared using the sol-immobilised method shows higher conversion of CO_2 towards methanol than the classic impregnation method. The sol immobilisation method provides an excellent way to control the mean particle size of Pd and PdZn particles after exposing the catalysts under a high temperature reductive environment. Both catalysts dried in air at 120 °C formed Pd nanoparticles with an average particle size of ~2–3 nm. Upon reduction, we observed transformation of Pd to the PdZn alloy beginning at ~250 °C. However, the IM catalysts show rapid growth of the PdZn particles to ~30 nm when reduced at 700 °C. In contrast the SI catalyst is much more stable with the PdZn diameter only increasing to ~7 nm when the catalyst was reduced at as high as 700 °C. Fig. 13 shows the influence of PdZn diameter on catalyst activity. It clearly shows that CO_2 conversion and methanol yield are strongly reliant on the PdZn particle size. We also illustrate the correlation between product selectivity and diameter of PdZn alloy (Fig. 14). It is clear that maintaining a small particle size is important for high methanol selectivity. Here there is a decrease in methanol selectivity from 60% at 3 nm size, down to 20% at 7 nm, and with the effective methanol turnover frequency diminishing from 5×10^{-4} metal site^{-1} s^{-1} to 7×10^{-5}.

In summary, Pd nanoparticles deposited via the sol immobilisation method produced active catalysts for methanol production where the key factor is the formation of PdZn alloy nanoparticles with controlled particle size. Methanol production increases at high Pd loadings for colloidal catalysts. PXRD and XPS analyses show the formation of a PdZn phase at reduction temperatures as low as 250 °C. PdZn bimetallic formation enormously enhances

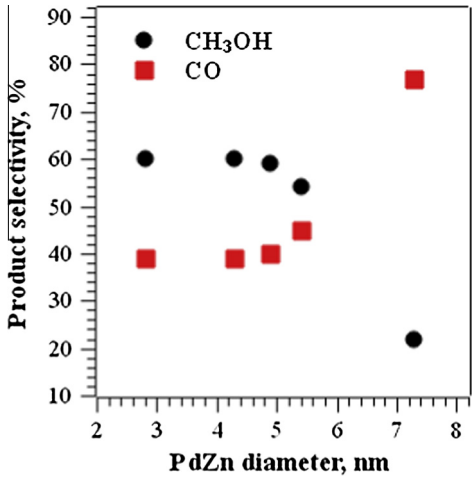

Fig. 14. Correlation between CO and CH_3OH selectivity with PdZn diameter for 5% Pd/ZnO prepared using sol immobilisation method. Reaction was carried out at 250 °C, 20 bar under the flow of 30 ml/min CO_2: $3H_2$. Catalytic activity was measured after 3 h reaction. All catalysts were pre-treated in situ at 400 °C with H_2 flow for 60 min, after calcination at different temperatures resulting in particle sintering.

CH_3OH production; however, reduction at higher temperature ~700 °C inhibits conversion, due to some sintering. The nature of the active site for CO_2 hydrogenation and RWGS reaction is different, as evidenced from the increased conversion of CO_2 to CH_3OH due to PdZn formation, but the presence of metallic Pd-only nanoparticles favours the RWGS reaction to make CO. Catalysts prepared via impregnation are poor, mainly due to residual Cl contamination and sintering.

Acknowledgments

The authors wish to acknowledge UK Catalysis Hub for research funding, the EPSRC for funding for Peter Wells, Wilm Jones, Liza Bahruji and Emma Gibson (EP/I019693/1, EP/K014714/1, EP/I038748/1, EP/K014854/1) and Diamond Light Source for provision of beamtime (SP10306) and the support of their staff. The RCaH are also acknowledged for use of facilities and support of their technical staff.

Appendix A. Supplementary material

Supplementary data associated with this article can be found, in the online version, at http://dx.doi.org/10.1016/j.jcat.2016.03.017.

References

[1] A. Behr, Methanol: the basic chemical and energy feedstock of the future, Asinger's vision today. Edited by Martin Bertau, Heribert Offermanns, Ludolf Plass, Friedrich Schmidt and Hans-Jürgen Wernicke, Angew. Chem. Int. Ed. 53 (2014) 12674.
[2] S. Lee, J.G. Speight, S.K. Loyalka, Handbook of Alternative Fuel Technology, CRS Press, Taylor & Francis Group, 2007.
[3] K. Roh, T.B.H. Nguyen, U. Suriyapraphadilok, J.H. Lee, R. Gani, Development of sustainable CO_2 conversion processes for the methanol production, in: J.K.H. Krist, V. Gernaey, G. Rafiqul (Eds.), Computer Aided Chemical Engineering, Elsevier, 2015, pp. 1145–1150.
[4] S. Lee, Methanol Synthesis Technology, Taylor & Francis, 1989.
[5] W. Wang, S. Wang, X. Ma, J. Gong, Recent advances in catalytic hydrogenation of carbon dioxide, Chem. Soc. Rev. 40 (2011) 3703–3727.
[6] F. Stone, D. Waller, Cu–ZnO and Cu–ZnO/Al2O3 catalysts for the reverse water-gas shift reaction. The effect of the Cu/Zn ratio on precursor characteristics and on the activity of the derived catalysts, Top. Catal. 22 (2003) 305–318.
[7] X. An, Y. Zuo, Q. Zhang, J. Wang, Methanol synthesis from CO_2 hydrogenation with a Cu/Zn/Al/Zr fibrous catalyst, Chin. J. Chem. Eng. 17 (2009) 88–94.
[8] M.J.L. Ginés, A.J. Marchi, C.R. Apesteguía, Kinetic study of the reverse water–gas shift reaction over $CuO/ZnO/Al_2O_3$ catalysts, Appl. Catal. A Gen. 154 (1997) 155–171.
[9] M.S. Spencer, The role of zinc oxide in Cu/ZnO catalysts for methanol synthesis and the water–gas shift reaction, Top. Catal. 8 (1999) 259–266.
[10] J. Nakamura, I. Nakamura, T. Uchijima, Y. Kanai, T. Watanabe, M. Saito, T. Fujitani, A surface science investigation of methanol synthesis over a Zn-deposited polycrystalline Cu surface, J. Catal. 160 (1996) 65–75.
[11] M. Behrens, F. Studt, I. Kasatkin, S. Kühl, M. Hävecker, F. Abild-Pedersen, S. Zander, F. Girgsdies, P. Kurr, B.-L. Kniep, M. Tovar, R.W. Fischer, J.K. Nørskov, R. Schlögl, The active site of methanol synthesis over $Cu/ZnO/Al_2O_3$ industrial catalysts, Science 336 (2012) 893–897.
[12] F. Studt, M. Behrens, E.L. Kunkes, N. Thomas, S. Zander, A. Tarasov, J. Schumann, E. Frei, J.B. Varley, F. Abild-Pedersen, J.K. Nørskov, R. Schlögl, The mechanism of CO and CO_2 hydrogenation to methanol over Cu-based catalysts, ChemCatChem 7 (2015) 1105–1111.
[13] S. Kuld, C. Conradsen, P.G. Moses, I. Chorkendorff, J. Sehested, Quantification of zinc atoms in a surface alloy on copper in an industrial-type methanol synthesis catalyst, Angew. Chem. Int. Ed. 53 (2014) 5941–5945.
[14] M. Behrens, Chemical hydrogen storage by methanol: challenges for the catalytic methanol synthesis from CO_2, in: Recycl. Catal., 2015.
[15] F. Studt, I. Sharafutdinov, F. Abild-Pedersen, C.F. Elkjær, J.S. Hummelshøj, S. Dahl, I. Chorkendorff, J.K. Nørskov, Discovery of a Ni–Ga catalyst for carbon dioxide reduction to methanol, Nat. Chem. 6 (2014) 320–324.
[16] J. Graciani, K. Mudiyanselage, F. Xu, A.E. Baber, J. Evans, S.D. Senanayake, D.J. Stacchiola, P. Liu, J. Hrbek, J.F. Sanz, J.A. Rodriguez, Highly active copper-ceria and copper-ceria-titania catalysts for methanol synthesis from CO_2, Science 345 (2014) 546–550.
[17] G. Prieto, J. Zečević, H. Friedrich, K.P. de Jong, P.E. de Jongh, Towards stable catalysts by controlling collective properties of supported metal nanoparticles, Nat. Mater. 12 (2013) 34–39.
[18] T. Inui, T. Takeguchi, Effective conversion of carbon dioxide and hydrogen to hydrocarbons, Catal. Today 10 (1991) 95–106.
[19] N. Iwasa, H. Suzuki, M. Terashita, M. Arai, N. Takezawa, Methanol synthesis from CO_2 under atmospheric pressure over supported Pd catalysts, Catal. Lett. 96 (2004) 75–78.
[20] S.E. Collins, J.J. Delgado, C. Mira, J.J. Calvino, S. Bernal, D.L. Chiavassa, M.A. Baltanás, A.L. Bonivardi, The role of Pd–Ga bimetallic particles in the bifunctional mechanism of selective methanol synthesis via CO_2 hydrogenation on a Pd/Ga_2O_3 catalyst, J. Catal. 292 (2012) 90–98.
[21] T. Fujitani, M. Saito, Y. Kanai, T. Watanabe, J. Nakamura, T. Uchijima, Development of an active Ga_2O_3 supported palladium catalyst for the synthesis of methanol from carbon dioxide and hydrogen, Appl. Catal. A Gen. 125 (1995) L199–L202.
[22] A. Ota, E.L. Kunkes, I. Kasatkin, E. Groppo, D. Ferri, B. Poceiro, R.M. Navarro Yerga, M. Behrens, Comparative study of hydrotalcite-derived supported Pd2Ga and PdZn intermetallic nanoparticles as methanol synthesis and methanol steam reforming catalysts, J. Catal. 293 (2012) 27–38.
[23] N. Koizumi, X. Jiang, J. Kugai, C. Song, Effects of mesoporous silica supports and alkaline promoters on activity of Pd catalysts in CO_2 hydrogenation for methanol synthesis, Catal. Today 194 (2012) 16–24.
[24] X.-L. Liang, X. Dong, G.-D. Lin, H.-B. Zhang, Carbon nanotube-supported Pd–ZnO catalyst for hydrogenation of CO_2 to methanol, Appl. Catal. B Environ. 88 (2009) 315–322.
[25] M. Friedrich, S. Penner, M. Heggen, M. Armbrüster, High CO_2 selectivity in methanol steam reforming through ZnPd/ZnO teamwork, Angew. Chem. Int. Ed. 52 (2013) 4389–4392.
[26] A. Karim, T. Conant, A. Datye, The role of PdZn alloy formation and particle size on the selectivity for steam reforming of methanol, J. Catal. 243 (2006) 420–427.
[27] M. Armbrüster, M. Behrens, K. Föttinger, M. Friedrich, É. Gaudry, S.K. Matam, H.R. Sharma, The intermetallic compound ZnPd and its role in methanol steam reforming, Catal. Rev. 55 (2013) 289–367.
[28] J. Vizdal, A. Kroupa, J. Popovic, A. Zemanova, The experimental and theoretical study of phase equilibria in the Pd–Zn (-Sn) system, Adv. Eng. Mater. 8 (2006) 164–176.
[29] C.-H. Kim, J. Lee, D.L. Trimm, The preparation and characterisation of Pd–ZnO catalysts for methanol synthesis, Top. Catal. 22 (2003) 319–324.
[30] A. Bansode, A. Urakawa, Towards full one-pass conversion of carbon dioxide to methanol and methanol-derived products, J. Catal. 309 (2014) 66–70.
[31] J. Toyir, P.R.r. de la Piscina, J.L.G. Fierro, N.s. Homs, Highly effective conversion of CO_2 to methanol over supported and promoted copper-based catalysts: influence of support and promoter, Appl. Catal. B Environ. 29 (2001) 207–215.
[32] X.-M. Liu, G.Q. Lu, Z.-F. Yan, Nanocrystalline zirconia as catalyst support in methanol synthesis, Appl. Catal. A Gen. 279 (2005) 241–245.
[33] X. An, J. Li, Y. Zuo, Q. Zhang, D. Wang, J. Wang, A Cu/Zn/Al/Zr fibrous catalyst that is an improved CO_2 hydrogenation to methanol catalyst, Catal. Lett. 118 (2007) 264–269.
[34] http://www.casaxps.com/.
[35] M. Newville, IFEFFIT: interactive XAFS analysis and FEFF fitting, J. Synchrot. Radiat. 8 (2001) 322–324.
[36] B. Ravel, M. Newville, ATHENA, ARTEMIS, HEPHAESTUS: data analysis for X-ray absorption spectroscopy using IFEFFIT, J. Synchrot. Radiat. 12 (2005) 537–541.
[37] H. Cheng, K. Scott, Selection of oxygen reduction catalysts for rechargeable lithium–air batteries—Metal or oxide?, Appl Catal. B Environ. 108–109 (2011) 140–151.
[38] T. Conant, A.M. Karim, V. Lebarbier, Y. Wang, F. Girgsdies, R. Schlögl, A. Datye, Stability of bimetallic Pd–Zn catalysts for the steam reforming of methanol, J. Catal. 257 (2008) 64–70.
[39] P.S. Wehner, G.C. Tustin, B.L. Gustafson, XPS study of the reduction and reoxidation of ZnO-supported palladium, J. Catal. 88 (1984) 246–248.
[40] J.A. Rodriguez, Interactions in bimetallic bonding: electronic and chemical properties of PdZn surfaces, J. Phys. Chem. 98 (1994) 5758–5764.
[41] L. Bollmann, J.L. Ratts, A.M. Joshi, W.D. Williams, J. Pazmino, Y.V. Joshi, J.T. Miller, A.J. Kropf, W.N. Delgass, F.H. Ribeiro, Effect of Zn addition on the water–gas shift reaction over supported palladium catalysts, J. Catal. 257 (2008) 43–54.
[42] B.R. Fingland, F.H. Ribeiro, J.T. Miller, Simultaneous measurement of X-ray absorption spectra and kinetics: a fixed-bed, plug-flow operando reactor, Catal. Lett. 131 (2009) 1–6.
[43] D.J. Childers, N.M. Schweitzer, S.M.K. Shahari, R.M. Rioux, J.T. Miller, R.J. Meyer, Modifying structure-sensitive reactions by addition of Zn to Pd, J. Catal. 318 (2014) 75–84.
[44] K. Fottinger, J.A. van Bokhoven, M. Nachtegaal, G. Rupprechter, Dynamic structure of a working methanol steam reforming catalyst. In situ quick-EXAFS on Pd/ZnO nanoparticles, J. Phys. Chem. Lett. 2 (2011) 428–433.
[45] A.M. Beale, B.M. Weckhuysen, Phys. Chem. Chem. Phys. 12 (2010) 5562–5574.
[46] J.K. Edwards, B.E. Solsona, P. Landon, A.F. Carley, A. Herzing, C.J. Kiely, G.J. Hutchings, Direct synthesis of hydrogen peroxide from H_2 and O_2 using TiO_2-supported Au–Pd catalysts, J. Catal. 236 (2005) 69–79.
[47] G.-X. Qi, X.-M. Zheng, J.-H. Fei, Z.-Y. Hou, Low-temperature methanol synthesis catalyzed over $Cu/\gamma\text{-}Al_2O_3\text{–}TiO_2$ for CO_2 hydrogenation, Catal. Lett. 72 (2001) 191–196.
[48] K.I. Hadjiivanov, G.N. Vayssilov, Characterization of oxide surfaces and zeolites by carbon monoxide as an IR probe molecule, in: Advances in Catalysis, Academic Press, 2002, pp. 307–511.
[49] R.J.H. Clark, R.E. Hester (Eds.), Advances in Infrared and Raman Spectroscopy, Heyden & Son, Philadelphia, Rheine, 1978, pp. 67–148.

[50] T. Lear, R. Marshall, J. Antonio Lopez-Sanchez, S.D. Jackson, T.M. Klapötke, M. Bäumer, G. Rupprechter, H.-J. Freund, D. Lennon, The application of infrared spectroscopy to probe the surface morphology of alumina-supported palladium catalysts, J. Chem. Phys. 123 (2005) 174706.
[51] K. Föttinger, G. Rupprechter, In situ spectroscopy of complex surface reactions on supported Pd–Zn, Pd–Ga, and Pd(Pt)–Cu nanoparticles, Acc. Chem. Res. 47 (2014) 3071–3079.
[52] M. Bowker, R.A. Hadden, H. Houghton, J.N.K. Hyland, K.C. Waugh, The mechanism of methanol synthesis on copper/zinc oxide/alumina catalysts, J. Catal. 109 (1988) 263–273.
[53] S.A. French, A.A. Sokol, S.T. Bromley, C.R.A. Catlow, P. Sherwood, Identification and characterization of active sites and their catalytic processes—the Cu/ZnO methanol catalyst, Top. Catal. 24 (2003) 161–172.
[54] K. Tedsree, T. Li, S. Jones, C.W.A. Chan, K.M.K. Yu, P.A.J. Bagot, E.A. Marquis, G.D. W. Smith, S.C.E. Tsang, Hydrogen production from formic acid decomposition at room temperature using a Ag–Pd core-shell nanocatalyst, Nat. Nanotech. 6 (2011) 302–307.
[55] N. Aas, L. Yongxue, M. Bowker, The adsorption and decomposition of formic acid on clean and oxygen-dosed Pd(110), J. Phys.: Condens. Matter 3 (1991) S281.
[56] A.M. Karim, T. Conant, A.K. Datye, Controlling ZnO morphology for improved methanol steam reforming reactivity, Phys. Chem. Chem. Phys. 10 (2008) 5584–5590.
[57] J. Saussey, J.-C. Lavalley, C. Bovet, Infrared study of CO_2 adsorption on ZnO. Adsorption sites, J. Chem. Soc. Faraday Trans. 1: Phys. Chem. Condens. Phases 78 (1982) 1457–1463.
[58] J. Koßmann, G. Roßmüller, C. Hättig, Prediction of vibrational frequencies of possible intermediates and side products of the methanol synthesis on ZnO ($000\bar{1}$) by ab initio calculations, J. Chem. Phys. 136 (2012).
[59] M. Bowker, H. Houghton, K.C. Waugh, Mechanism and kinetics of methanol synthesis on zinc oxide, J. Chem. Soc. Faraday Trans. 1: Phys. Chem. Condens. Phases 77 (1981) 3023–3036.
[60] D. Ehrlich, S. Wohlrab, J. Wambach, H. Kuhlenbeck, H.J. Freund, Reaction of CO_2 on Pd(111) activated via promotor action of alkali coadsorption, Vacuum 41 (1990) 157–160.
[61] J.A. Rodriguez, D.W. Goodman, The nature of the metal–metal bond in bimetallic surfaces, Science 257 (1992) 897–903.
[62] Q.-L. Tang, Q.-H. Luo, Adsorption of CO_2 at ZnO: a surface structure effect from DFT+U calculations, J. Phys. Chem. C 117 (2013) 22954–22966.
[63] A. Ota, M. Armbrüster, M. Behrens, D. Rosenthal, M. Friedrich, I. Kasatkin, F. Girgsdies, W. Zhang, R. Wagner, R. Schlögl, Intermetallic compound Pd2Ga as a selective catalyst for the semi-hydrogenation of acetylene: from model to high performance systems, J. Phys. Chem. C 115 (2011) 1368–1374.
[64] M. Armbrüster, K. Kovnir, M. Behrens, D. Teschner, Y. Grin, R. Schlögl, Pd−Ga intermetallic compounds as highly selective semihydrogenation catalysts, J. Am. Chem. Soc. 132 (2010) 14745–14747.
[65] J. Qu, X. Zhou, F. Xu, X.-Q. Gong, S.C.E. Tsang, Shape effect of Pd-promoted Ga_2O_3 nanocatalysts for methanol synthesis by CO_2 hydrogenation, J. Phys. Chem. C 118 (2014) 24452–24466.